



CFD Analysis for Merdeka 2 Solar Vehicle

Zahari Taha¹, Rossi Passarella^{2,5,*}, Sugiyono³, Nasrudin Abd Rahim²,
Jamali Md Sah⁴, and Aznijar Ahmad-Yazid²

¹Faculty of Manufacturing Engineering and Technology Management, Universiti Malaysia Pahang, 26300, Malaysia

²Faculty of Engineering, University of Malaya, Kuala Lumpur, 50603, Malaysia

³Department of Mechanical and Industrial Engineering, Gadjah Mada University, Yogyakarta, 55281, Indonesia

⁴School of Manufacturing Engineering, Universiti Malaysia Perlis, 02600, Malaysia

⁵Department of Computer Engineering, University of Sriwijaya, Palembang, 30662, Indonesia

Vehicle's low drag force is critical to achieve higher speed and for efficient energy usage. Most solar vehicles that participated in the World Solar Challenge event adopted the 'cockroach' shape which has been considered as the best shape to achieve optimum speed and aerodynamics characteristics. However, the team from University of Malaya decided to design their entry vehicle based on the profile of a box fish, said to possess an even lower drag coefficient value. This paper describes the aerodynamics characteristics numerical study of the solar vehicle using a computational fluid dynamics (CFD) code called FLUENT. The numerical computation is based on the frontal area of the vehicle and the obtained results have shown reasonable values of drag and lift coefficients when compared to ordinary road vehicles.

Keywords: Solar Vehicle, World Solar Challenge, Box Fish Shape, CFD.

1. INTRODUCTION

In 2009, the Center for Product Design and Manufacturing (CPDM) University of Malaya again participated in the World Solar Challenge (WSC) event with a second version of solar vehicle, named Merdeka 2; shown in Figure 1. The concept of using off-the-shelf components previously adopted for the first entrant in 2007, Merdeka was maintained. The Merdeka 2 was designed to be as similar possible to an ordinary vehicle except for the presence of solar panels at the roof of the vehicle. The vehicle main body structure was fabricated using aluminium alloy. The solar vehicle used a 48 V permanent magnet DC motor rotating at 3000 r.p.m. maximum. 4 units of 12 V deep cycle batteries were used to store the generated electrical energy from the photovoltaic solar panels, which in turn powered the motor. Each of the 12 V batteries were individually charged by separate solar panels. 4 units of Maximum Power Point Tracking (MPPT) acted as the solar panels charging controller. During the 2009 event, with the average speed of 45 km/h, Merdeka 2 managed to finish 590 km of the approximately 3020 km, the total race distance. This achievement is approximately a 100% improvement compared to the performance of the previous entrant, Merdeka. The total manufacturing cost was approximated at RM 50,000.00 (US\$ 15,000). In the future, with limited funding, it is foreseen that the researchers at CPDM will face a huge task to continue developing of the next solar vehicle

with the aim of completing the race, or to overhaul Merdeka 2 achievement.

2. AERODYNAMICS ANALYSIS

Initially, the design concept for Merdeka 2 was based on the profile of the box fish, similar to the Mercedes Benz minivan, shown in Figure 2. This shape is said to possess a low drag coefficient value, C_d , of approximately 0.06, that can lead to a 20% reduction of fuel consumption.

To analyze the aerodynamics of the solar vehicle, a numerical method using computational fluid dynamics (CFD) code called FLUENT² was performed. Generally, there are two steps involved when performing this, firstly preparing the computational domain and then conducting the numerical analysis. The first step, preparing the computational domain was carried out using Gambit, an integrated pre-processor of FLUENT to create the geometry of the model, generating the grid system and assigning the boundary conditions. The second step was carried out using the FLUENT processor, where the numerical model was set up and the computation performed to achieve the solution.

The geometry of the model is drawn using the existing dimensions of the solar vehicle. However, in order to obtain a numerically acceptable model, a simplified geometry of the solar vehicle was drawn instead and is shown in Figure 3. The length, width and height of the solar vehicle model were 4620 mm, 1395 mm and 1375 mm, respectively.

* Author to whom correspondence should be addressed.



Fig. 1. Merdeka 2 Solar vehicle.

To perform the aerodynamic analysis in FLUENT, the model of the solar vehicle was drawn as if it is at the center of a wind tunnel with air being drawn across the model. This is shown in Figure 4. The model is also positioned 140 mm above of the wind tunnel base, following the lowest floor position of the solar vehicle above the road. The wind tunnel dimension was 23290 mm long, 6975 mm wide, and 4792 mm high. For the boundary conditions, the velocity-inlet and the pressure outlet were used on the upstream and the downstream boundaries, respectively. The non-slip conditions were applied on the entire solar vehicle surfaces and on the walls of the wind tunnel.

The 3-D computational domain was then meshed using a hybrid meshing scheme which is a combination of hexahedral, tetrahedral and pyramidal grids. The total number of grids

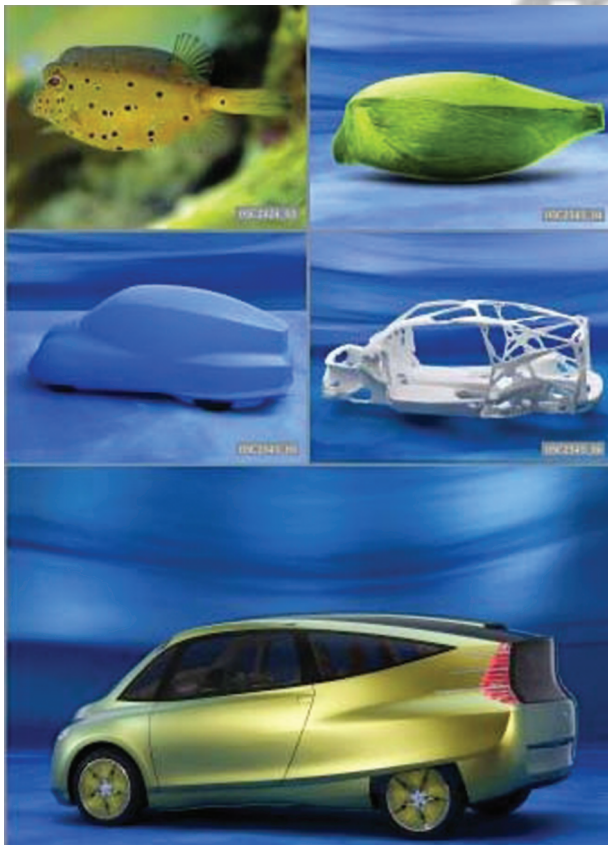


Fig. 2. The Mercedes Benz minivan based on the boxfish profile.

for the computational domain was approximately 1,100,000. Figure 5 shows the grid distribution on the surface of the solar vehicle model.

Afterwards, the computational domain of the model was numerically analyzed. The numerical model was set up in solving the governing Reynolds-averaged Navier-Stokes transport equations for conservation of mass and momentum.

The conservation of mass equation or continuity equation is

$$\frac{\partial \rho}{\partial t} + \frac{\partial}{\partial x_i}(\rho u_i) = 0 \quad (1)$$

While, the conservation of momentum equation is

$$\rho \frac{Du_i}{Dt} = -\frac{\partial p}{\partial x_i} + \frac{\partial}{\partial x_j} \left[\underbrace{\mu \left(\frac{\partial u_i}{\partial x_j} + \frac{\partial u_j}{\partial x_i} - \frac{2}{3} \delta_{ij} \frac{\partial u_k}{\partial x_k} \right)}_{\text{stress tensor}} \right] + \frac{\partial}{\partial x_j} \left(\underbrace{-\rho \overline{u'_i u'_j}}_{\text{Reynolds stresses}} \right) \quad (2)$$

The “Reynolds stresses” on the right-hand-side of Eq. (2) represents the effects of turbulence which must be modeled. A commonly employed method is the use of Boussinesq hypothesis to relate the Reynolds stresses to the mean velocity gradients, which is

$$-\rho \overline{u'_i u'_j} = \mu_t \left(\frac{\partial u_i}{\partial x_j} + \frac{\partial u_j}{\partial x_i} \right) - \frac{2}{3} \left(\rho k + \mu_t \frac{\partial u_k}{\partial x_k} \right) \delta_{ij} \quad (3)$$

Furthermore, additional transport equations were introduced in order to achieve “closure” Closure implies that there exist a sufficient number of equations to solve all the unknowns.

For this simulation, the turbulence is modeled using the Standard $k-\epsilon$ model, as prescribe by Lauder and Spalding.³ There are two additional transport equations that need to be solved; which are the turbulent kinetic energy (k) and the turbulence dissipation rate (ϵ). Both the variables of k and ϵ were then used to compute the turbulent viscosity (μ_t). Additionally, FLUENT documentation recommended that the non-equilibrium wall functions were employed for near-wall modeling by considering their ability to deal with complex flows involving separation, re-attachment, other non-equilibrium effects and strong pressure gradients.²

The turbulent kinetic energy (k) and the turbulence dissipation rate (ϵ) were obtained from the following transport equations:

$$\rho \frac{Dk}{Dt} = \frac{\partial}{\partial x_i} \left[\left(\mu + \frac{\mu_t}{\sigma_k} \right) \frac{\partial k}{\partial x_i} \right] + G_k + G_b - \rho \epsilon - Y_M \quad (4)$$

and

$$\rho \frac{D\epsilon}{Dt} = \frac{\partial}{\partial x_i} \left[\left(\mu + \frac{\mu_t}{\sigma_\epsilon} \right) \frac{\partial \epsilon}{\partial x_i} \right] + C_{1\epsilon} \frac{\epsilon}{k} (G_k + C_{3\epsilon} G_b) - C_{2\epsilon} \rho \frac{\epsilon^2}{k} \quad (5)$$

The turbulent viscosity was computed as follows:

$$\mu_t = \rho C_\mu \frac{k^2}{\epsilon} \quad (6)$$

In these equations, G_k represents the generation of turbulent kinetic energy due to the mean velocity gradients; G_b is the generation of turbulent kinetic energy due to buoyancy; Y_M represents the contribution of the fluctuating dilatation in compressible

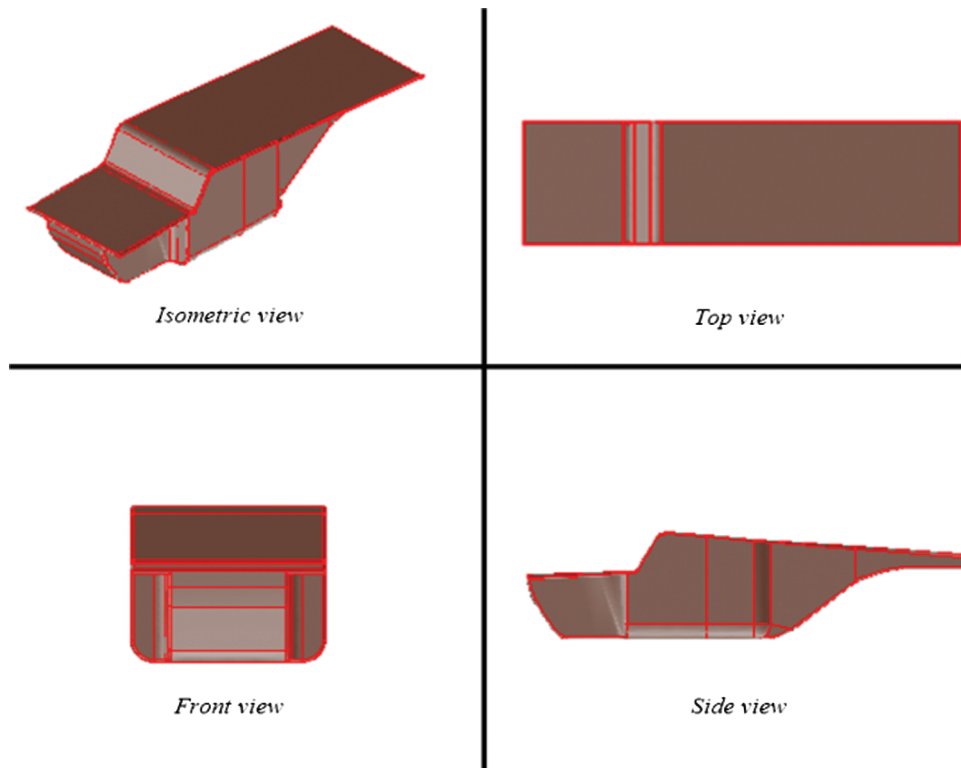


Fig. 3. Solar vehicle model.

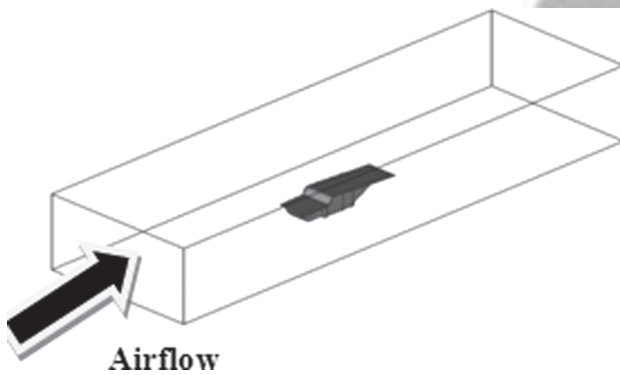


Fig. 4. Solar vehicle model in wind tunnel.

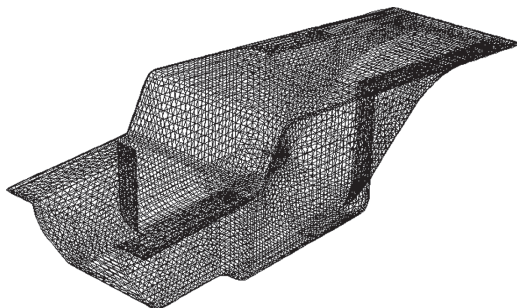


Fig. 5. Grids on surface of solar vehicle model.

turbulence to the overall dissipation rate; $C_{1\varepsilon}$, $C_{2\varepsilon}$, $C_{3\varepsilon}$, and C_{μ} are constants; σk and $\sigma\varepsilon$ are the turbulent Prandtl numbers for k and ε , respectively.

The governing equations were then solved sequentially which obeyed a solution algorithm called the segregated solver, shown

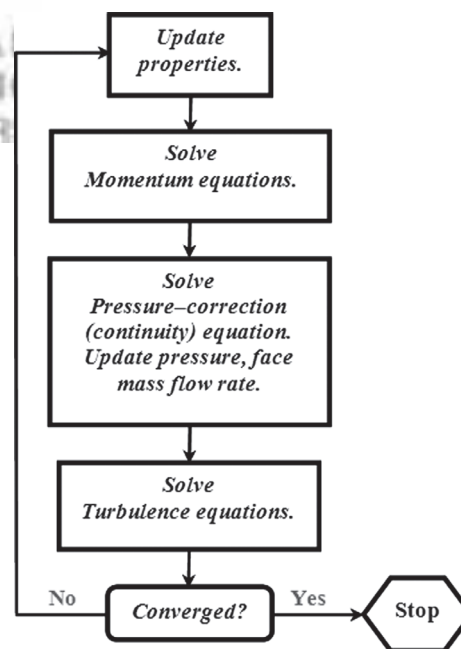


Fig. 6. Segregated solution algorithm. Reprinted with permission from [2], Fluent, Fluent 6.3 User's Guide, Fluent Inc.: Lebanon, NH (2006). © 2006.

Table I. The under-relaxation factors.

Variable	Under-relaxation factor
Pressure	0.3
Density	1
Body Force	1
Momentum	0.7
Turbulence kinetic energy	0.8
Turbulence dissipation rate	0.8
Turbulence viscosity	1

in Figure 6. Besides that, the governing equations were also discretized using the finite volume technique. In this calculation, the discretization schemes used are as follows: a standard scheme for the pressure; the SIMPLE algorithm for the pressure-velocity coupling; and the second-order accurate upwind scheme for the momentum, turbulent kinetic energy (k) and turbulence dissipation rate (ϵ). Furthermore, several iterations of the solution loop must be performed before a converged solution was obtained.

The calculation was carried out under steady flow condition at the inlet velocity value of 60 km/h, and the flow was modeled as incompressible. During the solution process, the default under-relaxation factors, shown in Table I were selected to control the update of computed variables, which was found to be

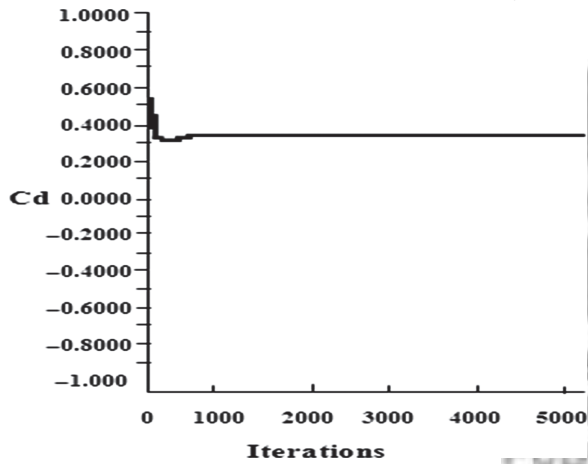


Fig. 7. Computational history of drag coefficient.

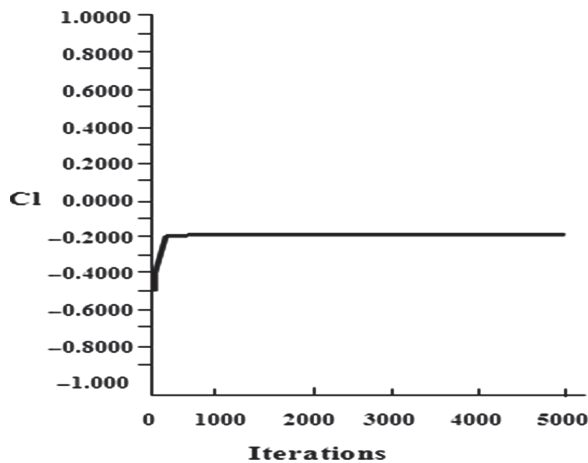


Fig. 8. Computational history of lift coefficient.

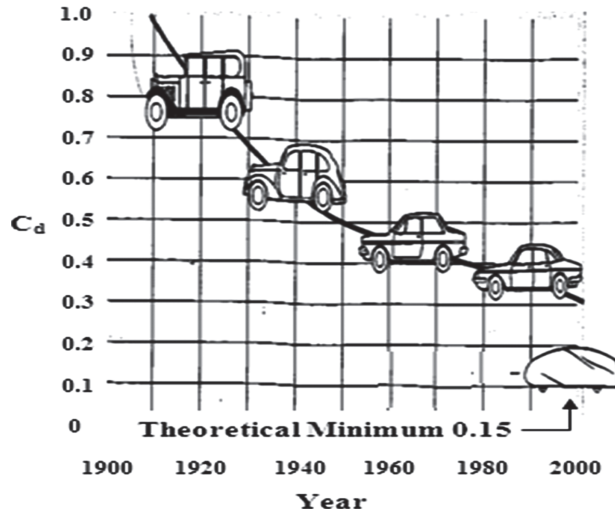


Fig. 9. Historical trend for drag coefficients of automobiles. Reprinted with permission from [4], Society of automotive engineers and SAE international congress and exposition, Vehicle aerodynamics: wake flows, computational fluid dynamics, and aerodynamic testing, Society of Automotive Engineers, Warrendale, PA (1992). © 1992.

near optimal for a large number of cases. The convergence of solution was monitored by checking the residuals of the numerically solved governing equations. Moreover, in order to properly scrutinize the convergence, the behavior of other quantities such as the drag coefficient (C_d) and the lift coefficient (C_l) were also monitored. For this analysis, the default convergence criterion of



Fig. 10. Existing Vehicles in the market with C_d 0.35.

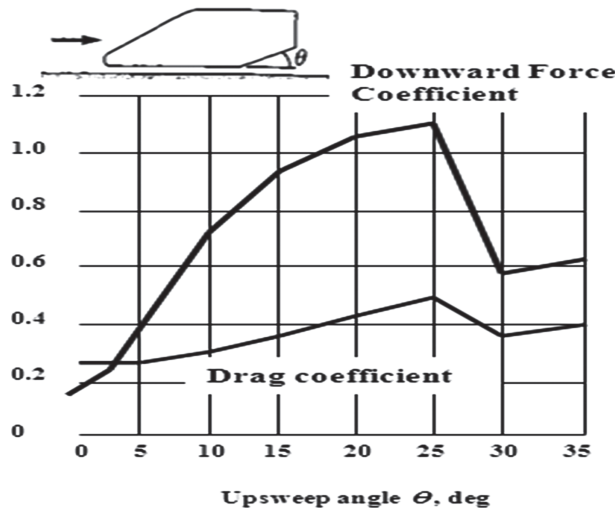


Fig. 11. Effect of bottom rear upsweep angle on drag and down-ward lift coefficients.

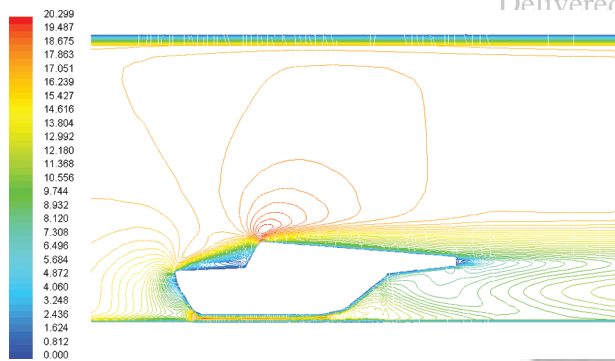


Fig. 12. Velocity contour of the airflow around the solar vehicle (m/s).

each residual was reduced to allow the monitored quantities to stagnate at consistent values.

3. SIMULATION RESULTS AND VALIDATION

Figures 7 and 8 show the computational history of drag and lift coefficients. The calculations are based on the frontal area of the solar vehicle. The consistent, converged value for drag coefficient was 0.35, while it was -0.19 for lift coefficient.

When compared with the drag coefficient values reflected by the historical drag coefficient automobile, shown in Figure 9 and with a couple of existing vehicle in the market, shown in Figure 10, the drag coefficient value obtained from the simulation seemed reasonable and commendable.

Furthermore, the designed Merdeka 2, with no upsweep angle exhibited a lift coefficient value of -0.19 (equal to downward force coefficient value of 0.19) which was also acceptable when compared to Bearman et al. findings, reproduced in Figure 11.⁶

Figure 12 shows the velocity contour of the airflow around the solar vehicle. It can be observed that low velocities existed at the front of the solar vehicle. This can be attributed to the stagnation condition of air flow at that location. Figure 13 confirmed this

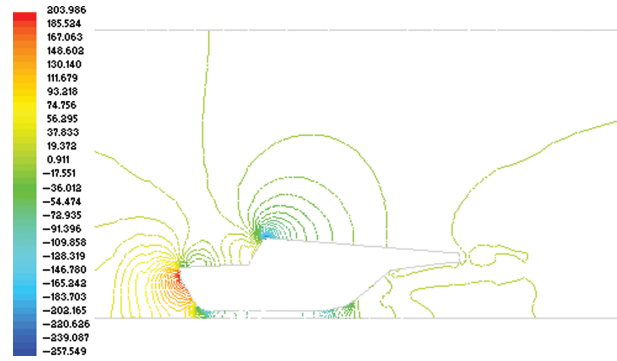


Fig. 13. Static pressure contour of the airflow around the solar vehicle (Pa).

observation by showing the highest static pressure noted at the front of the solar vehicle. Low velocities were also noted at the rear of the solar vehicle and at the front of the driver wind shield. These can be attributed to the formation of wake which created flow separation at those areas.

The C_d value obtained from the simulation was validated with experimental results conducted in Australia and was reported by Taha et al.⁷ This comparison was performed based on power consumption. The report indicated very slight difference in the theoretically calculated power at the speeds of 25, 36, and 60.7 km/h when compared with experimental values achieved. However there was no major difference at the maximum speed of 66.8 km/h.

4. CONCLUSION

Originally, the solar vehicle was designed based on the box fish shape. However, due to limited budget constrain and the requirement to adopt current off-the-shelf components used for the fabrication, the final Merdeka 2 shape was slightly different. The CFD analysis work of the Merdeka 2 solar vehicle was presented, with the simulation achieving the values of C_d and C_l at 0.35 and -0.19, respectively. There was also very slight difference between the simulated results obtained through FLUENT computation when compared with the experimental data.

References and Notes

- Mercedes-Benz bionic car modeled on boxfish. [Image on the Internet][updated 2005 June 7; Cited (2010) April 13] Available from: <http://www.dancewithshadows.com/auto/mercedes-benz-bionic-car-gallery.asp>.
- Fluent, Fluent 6.3 User's Guide, Fluent Inc.: Lebanon, NH (2006).
- B. E. Launder and D. B. Spalding, Lectures in Mathematical Models of Turbulence, Academic Press London, England (1972).
- Society of automotive engineers and SAE international congress and exposition, Vehicle aerodynamics: wake flows, computational fluid dynamics, and aerodynamic testing, Society of Automotive Engineers, Warrendale, PA (1992).
- Automobile drag Coefficients: WIKI.[Internet][Cited: (2010) April 15] Available from: http://wopedia.mobi/en/Automobile_drag_coefficients.
- P. W. Bearman, D. D. Beer, E. Hamidy, and J. K. Harvey, Society of Automotive Engineers Paper No. 880245 (1988) Int'l SAE Congress and Exposition, February-March. Detroit.
- Z. Taha, R. Passarella, N. A. Rahim, J. Md Sah, *ARPN J. Engineering and Applied Sciences* 5, 1 (2010).

Received: 20 June 2010. Accepted: 8 August 2010.